ChemPubSoc Europe

DOI: 10.1002/cphc.201600234

CHEMPHYSCHEM Articles

A Bis-Manganese(II)–DOTA Complex for Pulsed Dipolar Spectroscopy**

Paul Demay-Drouhard,[a] H. Y. Vincent Ching,[b] Dmitry Akhmetzyanov,[c] Régis Guillot,[d] Leandro C. Tabares,[b] Hélène C. Bertrand,*[a] and Clotilde Policar*[a]

High-spin gadolinium(III) and manganese(II) complexes have emerged as alternatives to standard nitroxide radical spin labels for measuring nanometric distances by using pulsed electron–electron double resonance (PELDOR or DEER) at high fields/frequencies. For certain complexes, particularly those with relatively small zero-field splitting (ZFS) and short distances between the two metal centers, the pseudosecular term of the dipolar coupling Hamiltonian is non-negligible. However, in general, the contribution from this term during conventional data analysis is masked by the flexibility of the molecule of interest and/or the long tethers connecting them to the spin labels. The efficient synthesis of a model system consisting of two $[Mn(dota)]^{2-}$ (MnDOTA; $DOTA^{4-}$ = 1,4,7,10-tetraazacyclododecane-1,4,7,10-tetraacetate) directly connected to the ends of a central rodlike oligo(phenylene–ethynylene) (OPE) spacer is reported. The rigidity of the OPE is confirmed by Q-band PELDOR measurements on a bis-nitroxide analogue. The Mn^{II}–Mn^{II} distance distribution profile determined by W-band PELDOR is in reasonable agreement with one simulated by using a simple rotamer analysis. The small degree of flexibility arising from the linking MnDOTA arm appears to outweigh the contribution from the pseudosecular term at this interspin distance. This study illustrates the potential of MnDOTA-based spin labels for measuring fairly short nanometer distances, and also presents an interesting candidate for in-depth studies of pulsed dipolar spectroscopy methods on Mn^{II}–Mn^{II} systems.

1. Introduction

Measuring nanometer-scale distances in biomacromolecules, such as proteins or nucleic acids, is an efficient way to unravel useful information about their structure and dynamics.[1–6] One of the ways this can be achieved is by using pulsed electron paramagnetic resonance (EPR) techniques, through which distances can be measured by determining the magnitude of magnetic dipolar coupling between pairs of paramagnetic centers.[7–9] The most commonly used method is pulsed electron–electron double resonance (PELDOR, also known as DEER).[10–13] PELDOR measurements with nitroxide radicals ($S = 1/2$), which can be incorporated into biomacromolecules through site-directed mutagenesis and spin labeling,[14,15] have been extensively studied;[7–9] most measurements are performed at X (9.5 GHz) and Q-band (34 GHz) frequencies.[16,17] Theoretically, the sensitivity of the measurement can be further improved by using higher fields/frequencies. However, the spectral width for organic radicals increases with field as their g anisotropy becomes resolved, which potentially provides information on orientations,[18–20] but can also reduce the expected sensitivity gain and complicate data analysis.[21] Furthermore, commonly used nitroxide radicals, such as (*S*)-(1-oxyl-2,2,5,5-tetramethyl-2,5-dihydro-1*H*-pyrrol-3-yl)methyl methanesulfonothioate (MTSL) and (2,2,6,6-tetramethyl piperidin-1-yl)oxyl (TEMPO) derivatives, can be readily converted into EPR-silent *N*-hydroxylamines in the reducing environment of a cell;[22] this complicates PELDOR measurements in complex cellular environments.

In the last decade, high-spin gadolinium(III) ($S = 7/2$) and manganese(II) ($S = 5/2$) complexes have emerged as attractive alternatives.[23–28] At higher fields, the main feature in their EPR spectra is the $|-1/2> \rightarrow |+1/2>$ "central transition". The spectral width of this transition is proportional to D^2/ν_0, in which D is the size of the zero-field splitting (ZFS), assuming the asymmetry parameter E is equal to zero, and ν_0 is the spectrometer frequency. Consequently, unlike radicals, the spectral width of the Gd^{III} or Mn^{II} central transition becomes narrower and better resolved as the observation frequency increases. Furthermore,

[a] Dr. P. Demay-Drouhard, Dr. H. C. Bertrand, Prof. C. Policar
Ecole Normale Supérieure—PSL Research University
Département de Chimie, Sorbonne Universités—UPMC Univ Paris 06
CNRS UMR 7203 LBM, 24 rue Lhomond
75005 Paris (France)
E-mail: helene.bertrand@ens.fr
clotilde.policar@ens.fr

[b] Dr. H. Y. V. Ching, Dr. L. C. Tabares
Institute for Integrative Biology of the Cell (I2BC)
Department of Biochemistry, Biophysics and Structural Biology
Université Paris-Saclay, CEA, CNRS UMR 9198
Gif-sur-Yvette, F-91198 (France)

[c] D. Akhmetzyanov
Goethe-University Frankfurt am Main
Institute of Physical and Theoretical Chemistry and
Center for Biomolecular Magnetic Resonance
Max von Laue Str. 7, 60438 Frankfurt am Main (Germany)

[d] Dr. R. Guillot
Institut de Chimie Moléculaire et des Matériaux O'Orsay
Université Paris-Sud, UMR CNRS 8182, Université Paris-Saclay
91405 Orsay (France)

[**] $DOTA^{4-}$ = 1,4,7,10-tetraazacyclododecane-1,4,7,10-tetraacetate

Supporting Information for this article can be found under: http://dx.doi.org/10.1002/cphc.201600234.

these metal centers are generally stable within biological environments. Gd^{III}–Gd^{III} PELDOR distance measurements at Q (34 GHz) and W-band (95 GHz) frequencies have been performed in vitro on synthetic model compounds,[29–31] proteins,[32–35] peptides,[36,37] and DNA,[38] and also on proteins,[39] peptides,[40] and DNA[41] inside cells. Mn^{II} centers, which have received much less attention, are very promising in a biological context because Mn^{II} is endogenous in biological environments and present at the active site of numerous enzymes.[42] Mn^{II} can also replace Mg^{II} in other biomacromolecules due to similarities in size and charge.[43] Unlike Gd^{III}, the central transition of Mn^{II} centers is split into a sextet by the hyperfine interaction to the ^{55}Mn nucleus ($I = 5/2$), which reduces the sensitivity of Mn^{II}–Mn^{II} PELDOR measurements by a factor of six if D values are comparable.[26] However, this is partially compensated for by the lower spin multiplicity of Mn^{II} compared with that of Gd^{III}.[26] To date, only three Mn^{II}–Mn^{II} PELDOR studies have been reported and all were performed at the W-band frequency.[26–28] In the first instance, the distance between two $[Mn(edta)]^{2-}$ (MnEDTA; $EDTA^{4-}$ = ethylenediaminetetraacetate) derivatives, grafted through a disulfide tether onto cysteine residues of a protein fragment, was measured.[26] The dipolar modulation depth (λ), an important sensitivity parameter, was found to be low (0.4%), and this was attributed to the large D value ($D = 3000$ MHz) of MnEDTA. Recently, Martorana et al. reported the attachment of $[Mn(pedta)]^{-}$ derivatives (MnPEDTA; $PEDTA^{3-}$ = *N*-(pyrid-2-ylmethyl)ethylenediamine-*N*,*N*′,*N*′-triacetate) to cysteine residues of ubiquitin mutants through C–S conjugation.[28] For two of the derivatives, the D values were 1860(900) and 3060(600) MHz; the values in parentheses denote their distributions. As expected, in the corresponding Mn^{II}–Mn^{II} PELDOR measurements, λ values ($\approx$0.7–1%), which were comparable to or somewhat greater than that of MnEDTA, were observed. However, in contrast to MnEDTA, narrow distance distribution profiles, down to 0.6 nm full-width at half-height (fwhh), were observed in the MnPEDTA measurements; this was attributed to the short length and rigidity of the tether connecting the spin label to the protein.[28] Previously, we reported the grafting of two $[Mn(dota)]^{2-}$ (MnDOTA; $DOTA^{4-}$ = 1,4,7,10-tetraazacyclododecane-1,4,7,10-tetraacetate; $D = 280(150)$ MHz) derivatives through a flexible succinimidyl thioether tether onto a series on polyproline spacers.[27] The PELDOR measurements gave higher λ values (1.2 to 2%) and the Mn–Mn distance distributions were in good agreement with those obtained from molecular dynamics simulations. However, under certain acquisition conditions, additional features in the frequency-domain spectra became apparent and they were attributed to contributions from the pseudosecular term of the dipolar coupling Hamiltonian, which was found to be non-negligible for MnDOTA.[27] Similar observations have also been reported for Gd^{III}–Gd^{III} PELDOR measurements,[30] for which they were found to be more apparent for shorter interspin distances (< 3.4 nm). Thus, conventional application of Tikhonov regularization, as implemented in the DeerAnalysis toolbox,[44] which disregards the contribution from the pseudosecular term,[45] resulted in extra peaks in and/or broadening of the distance distribution profiles.[30] However, for MnDOTA, these effects were mostly obscured by the intrinsic flexibility of the macromolecules and/or the tether to the metal spin label.[27] In contrast, the pseudosecular term contributions were expected to be much smaller for MnEDTA and MnPEDTA due to their larger and more distributed D values.[28]

Taken together, it appears that a compromise between ZFS parameters, their distribution, and flexibility needs to be reached for Mn^{II} spin labels. However, despite the shortcomings of MnDOTA in specific cases, spin labels based on this motif are still very promising for biological Mn^{II} PELDOR and other pulsed dipolar EPR spectroscopic distance measurements because of sensitivity and stability[46] considerations. To assess the limitations of MnDOTA, in particular, at shorter and less flexible distances, we present herein the preparation and characterization of a water-soluble Mn^{II}–Mn^{II} complex with an expected Mn–Mn distance of around 2.5 nm, in which the chelating DOTA ligands have been directly attached to the backbone of a rigid oligo(phenylene–ethynylene) (OPE)[30,45,47–54] spacer through amide bonds. A bis-nitroxide analogue was also synthesized to evaluate the size and flexibility of the OPE spacer in the bis-Mn^{II} complex. PELDOR measurements performed on both systems are discussed.

2. Results

2.1. Synthesis of the Target Compounds

A convergent synthesis of symmetric OPE spacers containing alternate phenyl rings with and without small polyethyleneglycol (PEG) chains (diethyleneglycol methyl ether), which were introduced to improve water solubility, was devised by a double Sonogashira coupling between a *para*-substituted ethynylbenzene and a central diiodinated building block equipped with the PEG chains, which was synthesized in three steps. Compound **2**, prepared by tosylation of diethylene glycol monomethyl ether **1**,[55] was reacted with hydroquinone in a double Williamson reaction to afford the intermediate **3** in good yield.[56] Subsequent diiodination of **3** by using iodine in conjunction with KIO_3 in acetic acid afforded the diiodo building block **4** in satisfactory yield after recrystallization.[57] This protocol has been scaled up and provides an easy access to grams (30 g) of intermediate **4** (Scheme 1).

A double Sonogashira coupling between **4** and commercially available *p*-ethynylaniline (**5**), by using $[Pd(PPh_3)_2Cl_2]$ (0.1 equiv) and CuI (0.2 equiv) in a mixture of triethylamine/THF (1:1), afforded the dicoupled product **6** (OPE-diNH_2) in modest yield (52%; Scheme 2). To functionalize both extremities of this spacer with DOTA macrocycles, OPE-diNH_2 **6** was reacted with bromoacetyl bromide in the presence of K_2CO_3 to afford bromide **7**, which was subjected to double nucleophilic substitution with tri-*t*Bu-DO3A under classical conditions,[58–63] providing the *t*Bu-protected bis-DOTA compound **8** in good yield after column chromatography (Scheme 2).

Removal of the *t*Bu ester protecting groups of compound **8** was attempted under several conditions [1:1 trifluoroacetic acid (TFA)/CH_2Cl_2 with or without scavengers,[59] HCO_2H at

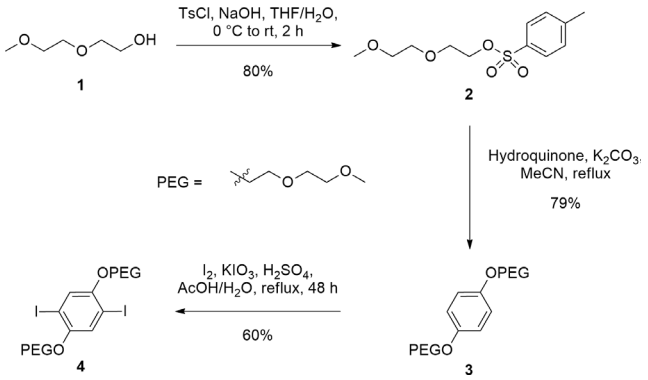

Scheme 1. Synthesis of the diiodo building block **4**. TsCl = 4-toluenesulfonyl chloride.

60 °C,[64] 6 M aqueous solution of HCl]; however, complex mixtures of unidentified products were obtained in each attempt (see HPLC profiles in Figure S1 in the Supporting Information). This deprotection step has been described to proceed smoothly, even on related compounds,[60] although low yields have sometimes been reported.[59] We surmised that the strong acidic conditions needed for the removal of the *t*Bu esters from the DOTA moieties, which is known to be sluggish,[65,66] led to the decomposition of compound **8**.

We turned our attention to the use of the more acid-labile phenylisopropyl (Pp) protecting group described by Mier et al.,[67] which could be cleaved in the presence of 2% TFA in CH_2Cl_2.[68] The Pp group has been successfully employed to generate peptides that incorporate a DOTA core with a much cleaner HPLC profile after cleavage from the resin than with the standard *t*Bu-protected DOTA.[66] Tri-Pp-DO3A **11** was synthesized in two steps from 2-phenyl-2-propanol **9** by treatment with bromoacetic acid in the presence of *N*,*N*′-dicyclohexylcarbodiimide (DCC) and 4-dimethylaminopyridine (DMAP) to give intermediate **10**, followed by reaction with 1,4,7,10-tetraazacyclododecane (cyclen; 0.33 equiv). Despite the low yield due to the concomitant formation of diversely alkylated cyclen derivatives as side products, tri-Pp-DO3A **11** was easily purified and obtained on a gram scale (Scheme 3).

The reaction between tri-Pp-DO3A **11** and bromide **7** under the conditions described above provided the Pp-protected bis-DOTA module **12**, which was cleanly deprotected in 4 h with a 2:2:96 TFA/TIS/CH_2Cl_2 cleavage cocktail, as monitored by reversed-phase HPLC (Figure S2 in the Supporting Information). The bis-DOTA-OPE model system **13** was obtained in high purity after purification by reversed-phase HPLC (Scheme 3). Due to the presence of the small PEG chains and the DOTA moieties, bis-DOTA-OPE **13** was very soluble in H_2O. The corresponding Mn^{II} complex (labeled $MnDOTA_2OPE$) was generated in situ by the addition of 1.8 equivalents of $Mn(ClO_4)_2$ to a buffered solution [4-(2-hydroxyethyl)-1-piperazineethanesulfonic acid (HEPES) 100 mM, pH 8] of **13** with 20% v/v glycerol.

The bis-TEMPO derivative **19** was also prepared by adopting a similar overall strategy. Commercially available *p*-bromobenzaldehyde (**14**) was reacted with trimethylsilylacetylene (TMSA) under Sonogashira coupling conditions to give intermediate **15** in good yield. The TMS group was then removed with K_2CO_3 in MeOH to afford *p*-ethynylbenzaldehyde **16**.[69] A double Sonogashira coupling between this compound and building block **4** gave OPE-diCOH **17** in 80% yield; compound **17** was oxidized with Oxone to generate the corresponding di-

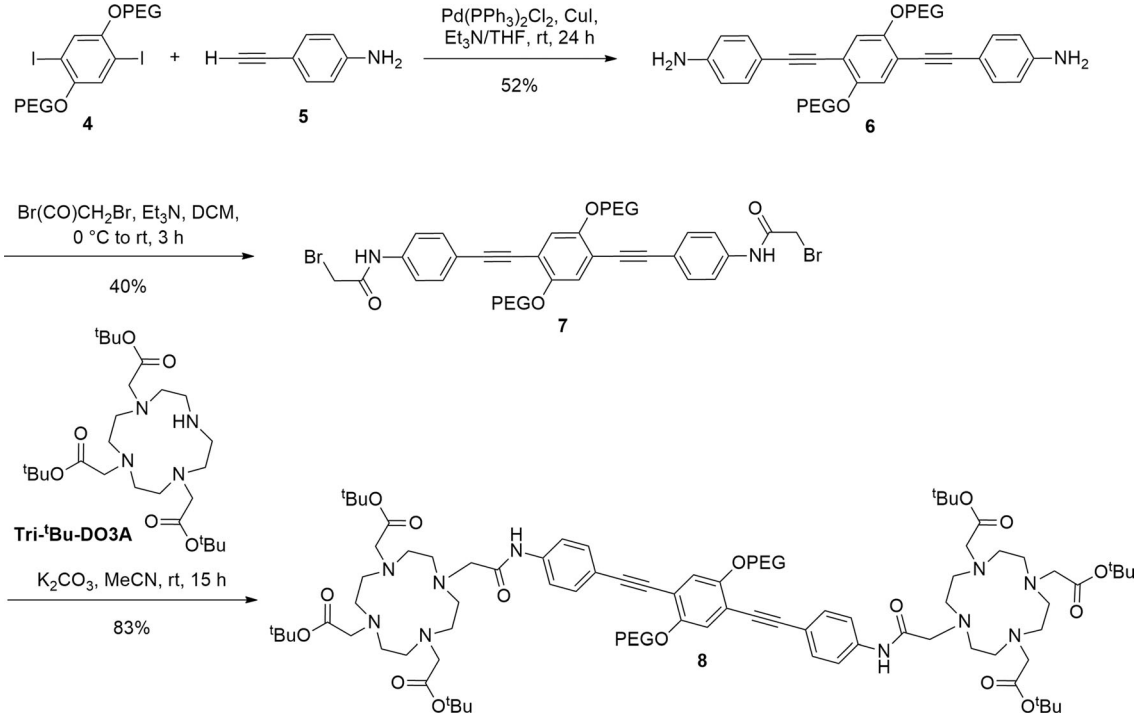

Scheme 2. Synthesis of the *t*Bu-protected bis-DOTA **8**.

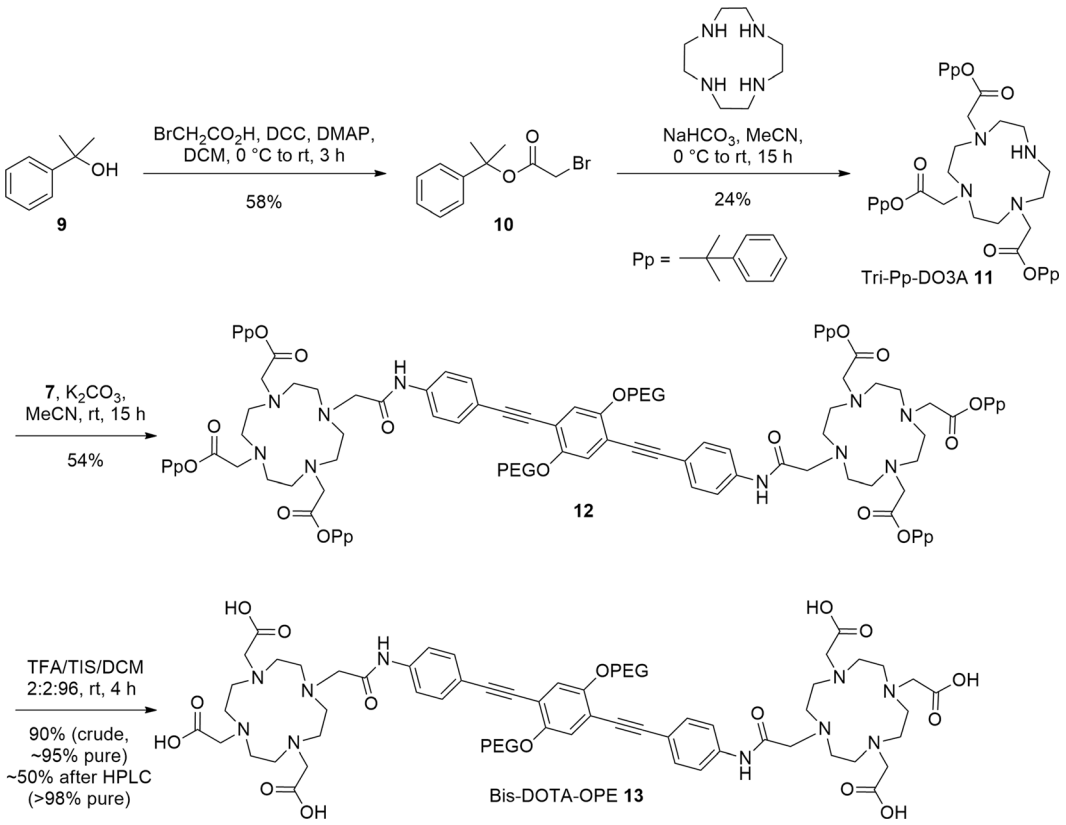

Scheme 3. Synthesis of the bis-DOTA-OPE **13**. TIS = triisopropylsilane.

carboxylic acid **18**. Amide-bond formation between OPE-diCO_2H **18** and commercially available 4-NH_2-TEMPO in the presence of DCC and 1-hydroxybenzotriazole (HOBt) gave bis-TEMPO-OPE **19** in excellent yield (Scheme 4). Interestingly, the yield obtained with this method was higher than those of standard coupling methods used to build systems incorporating two nitroxide radicals connected to a central rigid rod through ester bonds (usually in the region of 20%).[70]

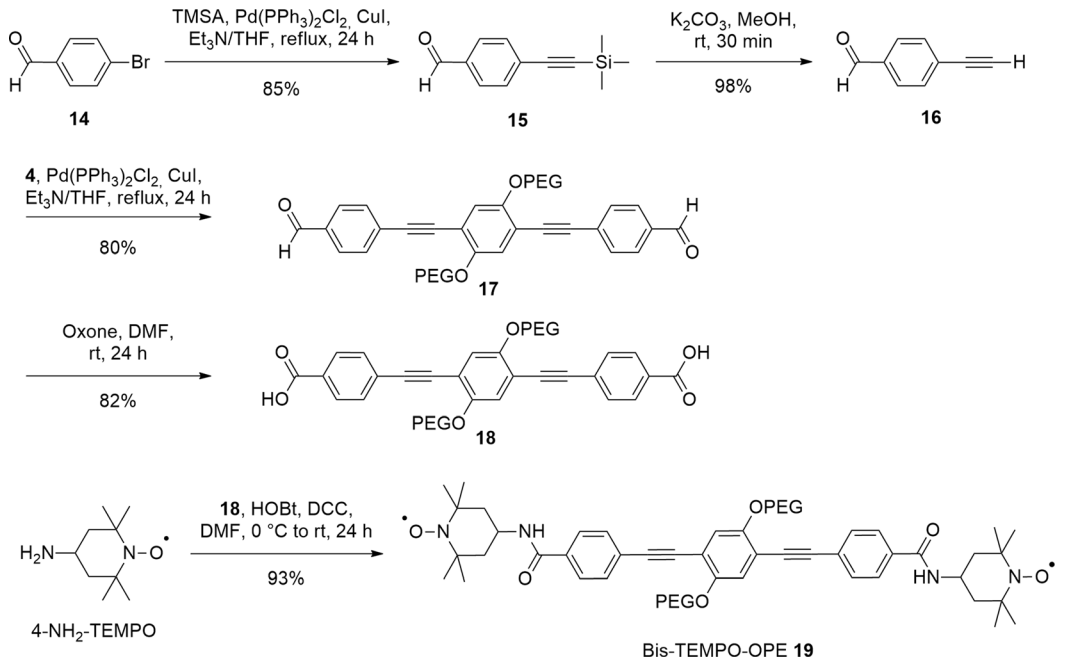

Scheme 4. Synthesis of the bis-TEMPO-OPE **19**.

2.2. X-ray Crystallography

Orange crystals of OPE-diCOH **17** suitable for XRD were obtained by slow evaporation from a 1:1 mixture of chloroform/ethyl acetate. Compound **17** crystallized in the $P\bar{1}$ space group (triclinic system). The aromatic rings were twisted relative to each other with dihedral angles of 18 and 31° relative to the central ring. The molecules were slightly bent (approximately 7°), which reflected the nonideal unidirectional arrangement of OPE spacers. No π stacking is observed, presumably because of the steric hindrance imposed by the PEG chains (Figure 1 A). The length of the OPE spacer (the C–C distance between the carbon atoms of the two aldehydes) was 1.93 nm.

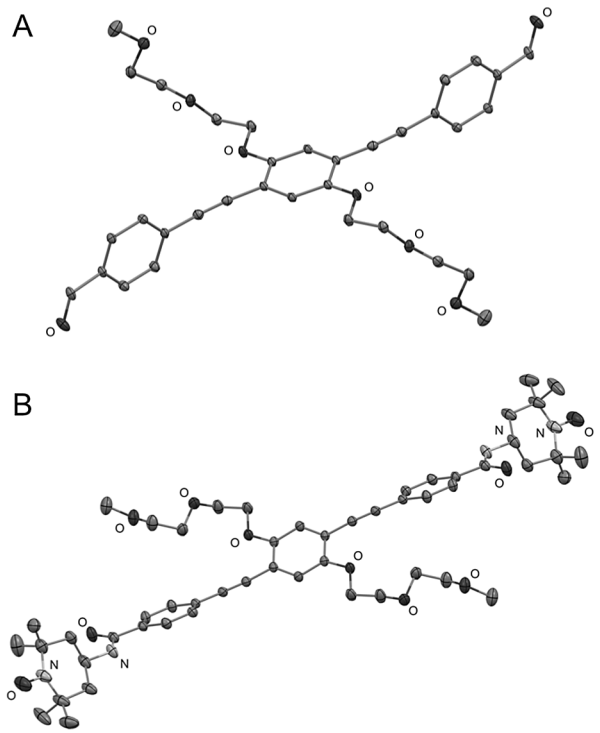

Figure 1. CSD Mercury[71] ellipsoid views of the structure of OPEs A) compound **17** and B) bis-TEMPO-OPE **19**. Ellipsoids are drawn at the 30% probability level.

Orange prisms of bis-TEMPO-OPE **19** were obtained by slow evaporation from a solution of the biradical in toluene. Compound **19** crystallized in the $P2_1/n$ space group (monoclinic system), with the three aromatic rings twisted by 39° from each other. The distance between the two N–O bonds (point-dipole approximation) was 3.02 nm (Figure 1 B) and the length of the OPE spacer (the distance between the two carbons of the amide bonds) was 1.93 nm, which was identical to that in OPE-diCOH **17** (Figure 1 B).

2.3. EPR Measurements

The W-band Hahn echo-detected field-swept EPR spectrum of $MnDOTA_2OPE$ in frozen glassy solution is depicted in Figure 2 A. A narrow sextet corresponding to the central transition superposing a broad component arising from the other transitions was observed, and was essentially the same as that of MnDOTA and MnDOTA-grafted polyprolines.[27] PELDOR measurements were performed with the pump pulse frequency (ν_{pump}) resonant with the highest field hyperfine line and the detection pulses frequency (ν_{detect}) set 70 MHz lower (Fig-

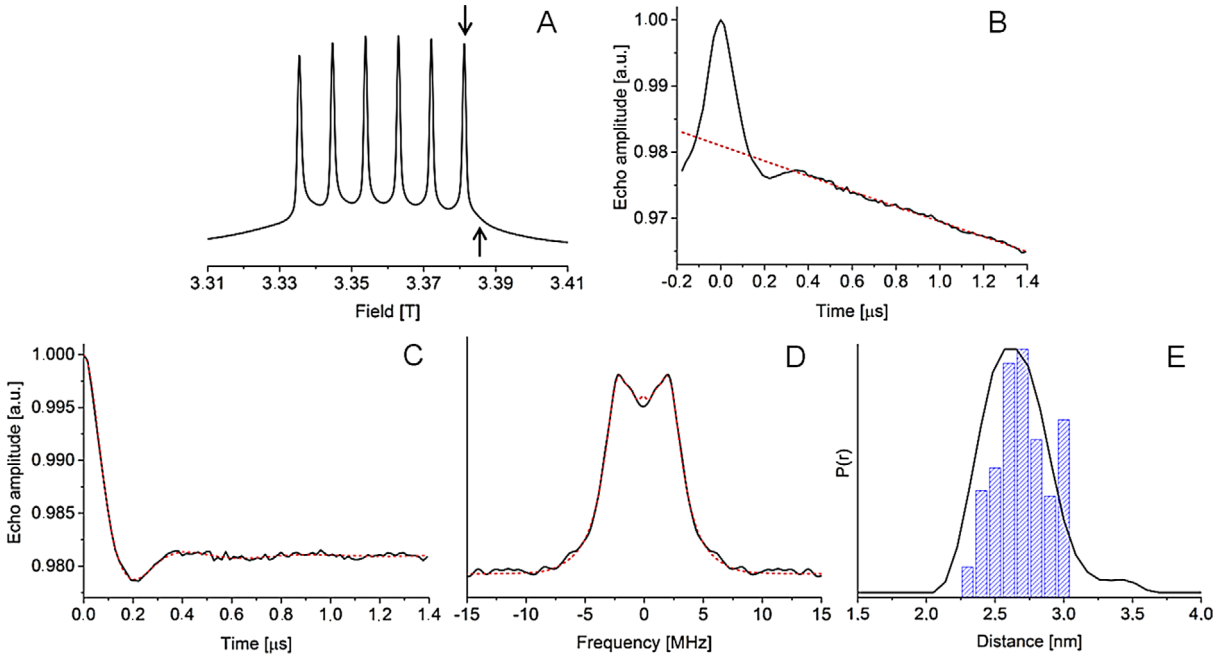

Figure 2. W-band PELDOR measurements on $MnDOTA_2OPE$ (100 μM) in HEPES (100 mM, pH 8) with 20% v/v glycerol at 10 K (black). A) Hahn echo-detected field-swept EPR spectrum with the pump and detection positions indicated schematically by the down and up arrows, respectively. B) Raw PELDOR time trace and background (dashed red). C) Background-corrected PELDOR time trace and its fit based on Tikhonov regularization (dashed red). D) Frequency-domain spectra corresponding to the experimental background-corrected time trace and its fit based on Tikhonov regularization (dashed red). E) Distance distribution profiles obtained by Tikhonov regularization and predicted by rotamer analysis (blue).

ure 2B–E). These frequency positions were chosen because previous studies suggested that the contribution from the pseudosecular term of the dipolar coupling Hamiltonian was least apparent when pumping at the hyperfine line and detecting off to the side.[27] The first modulation was clearly visible in the raw time trace and after background division the λ value was 1.9%, which was comparable to previous PELDOR measurements with MnDOTA.[27] The corresponding frequency-domain spectra showed a doublet with a splitting of 2.0 MHz. Tikhonov regularization, as conventionally implemented in DeerAnalysis,[44] gave a most probable distance of 2.6 nm. The fwhh of the distribution was 0.6 nm, which was comparable to the narrowest distance distribution profile observed in Mn^{II}–Mn^{II} PELDOR measurements.[28]

The Q-band Hahn echo-detected field-swept EPR spectrum of bis-TEMPO-OPE **19** is depicted in Figure 3A. PELDOR time traces (Figure 3B) were recorded across the whole EPR spectrum by using a constant $\nu_{detect}-\nu_{pump}$ offset of 50 MHz, with the exception of the magenta time trace for which an offset of −50 MHz was used. In the time traces, up to 7 full periods of a dampened dipolar oscillation were observed with modulation depths of up to 24%. Differences between the traces clearly indicate orientation selection.[19–21,72–76] For the orange and green time traces, the detection pulses were resonant with the lower field edge of the EPR spectrum, in which the g_{xx} component of the g tensor had a relatively large contribution to the excited orientations. In these two traces and their corresponding frequency domain spectra (Figure 3C), a large 3.6 MHz frequency component was observed. In contrast, for the other time traces, the main frequency component was at about 1.85 MHz. The orientation selection effects can be qualitatively rationalized in terms of the geometry of the biradical from its X-ray crystal structure. The g tensor of the nitroxide moieties is oriented with the g_{xx} component collinear to the mean axis of the molecule. For the orange and green time traces, the detection pulses sampled significant amounts of the g_{xx} component, such that the parallel orientation of the dipolar coupling tensor was excited to a high extent, which resulted in oscillations that were doubled in frequency (3.6 MHz) relative to the major component of the other time traces. In the green time trace, increased contributions from the g_{yy} and g_{zz} components meant that a single frequency (1.85 MHz) component was also observed. For all other time traces, the g_{xx} component only had a minor contribution to the signal, which resulted in time traces that lacked the parallel orientation of the dipolar coupling tensor. As expected, orientation selection was also observed at W-band frequencies (see Figure S4 in the Supporting Information).

The orientation selection effects were minimized by summing the Q-band PELDOR time traces (Figure 3D–F), which, in effect, provided a more uniform excitation of the dipolar coupling tensor orientations. The corresponding frequency domain spectrum resembled a complete Pake pattern. The summed time trace was analyzed by means of Tikhonov regu-

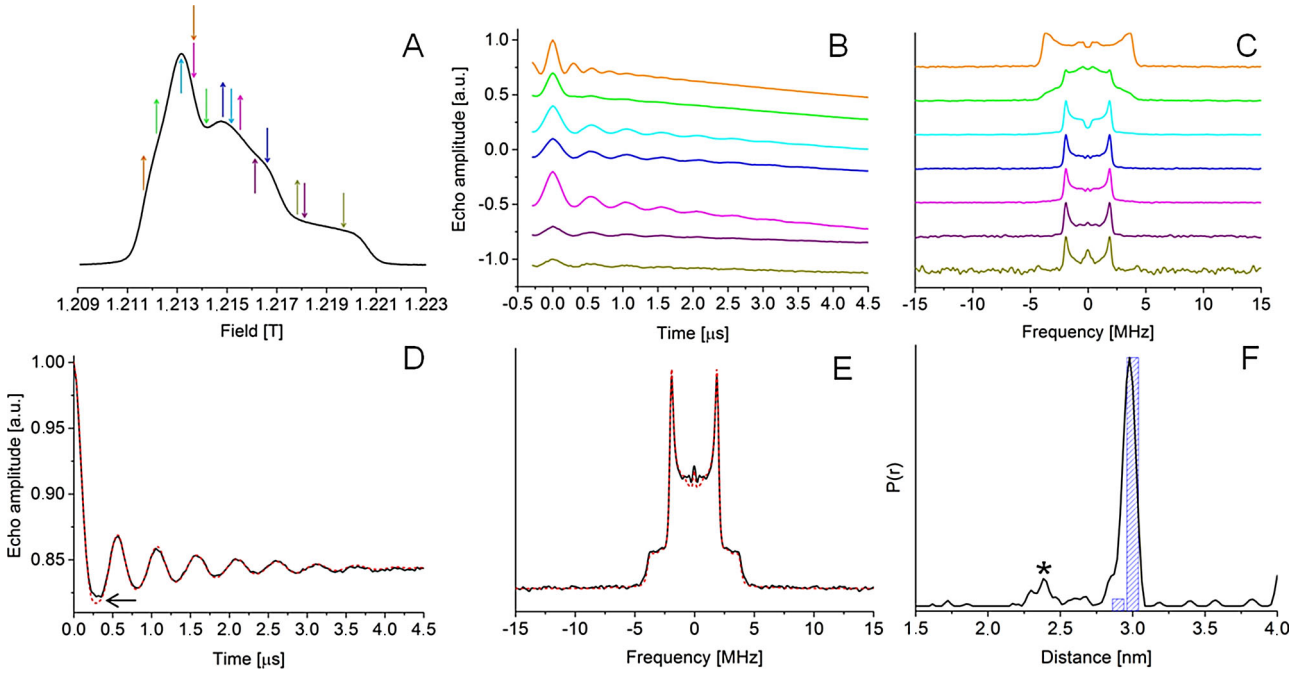

Figure 3. Q-band PELDOR measurements on bis-TEMPO-OPE **19** (100 µM) in 1:1 v/v [D_8]toluene/$CDCl_3$ at 50 K. A) Hahn echo-detected field-swept EPR spectrum with different pump and detection PELDOR positions indicated schematically in different colors by the down and up arrows, respectively. B) Raw PELDOR time traces recorded at different positions of the EPR spectrum, with colors corresponding to the arrows depicted in A). C) Fourier transform of the background-corrected time traces. D) The summed PELDOR time trace (black) after background correction and its fit based on Tikhonov regularization (dashed red), as implemented in DeerAnalysis.[40] The black arrow indicates a deviation due to imperfections of averaging of the orientation selection (discussed in detail in the text). E) Frequency-domain spectra corresponding to the background-corrected summed time trace (black) and its fit based on Tikhonov regularization (dashed red). F) Distance distribution profile obtained by Tikhonov regularization analysis of the summed PELDOR time trace and predicted by rotamer analysis (blue). The black asterisk indicates an artefact due to imperfection of averaging of orientation selection (details described in the text).

larization (Figure 3D–F). Small differences can be seen between the summed time trace (black) and the fit based on Tikhonov regularization (red), for example, at the first minimum of the dipolar oscillations, indicated with a black arrow in Figure 3D. This indicates that orientation selection is still present in the averaged time trace that gives rise to the small peak seen at 2.4 nm in Figure 3F. However, such imperfections are not expected to cause a significant error in the position of the main peak and the distance distribution. The most probable distance observed from the Tikhonov fit of the summed trace was 2.98 nm with a fwhh of 0.1 nm and width at 10% height of 0.2 nm.

2.4. Simulations of Distance Distribution Profiles

The Mn–Mn distance was simulated by using a rotamer analysis that accounted for the inherent flexibility of spin labels. This approach has been used to adequately predict distance distributions obtained from PELDOR measurements.[27,40,77–79] Starting from known X-ray crystal structures, we constructed a model of $MnDOTA_2OPE$ (Figure 4). Subject to certain constraints (see the Experimental Section), all possible rotamers that avoided clashes were generated and each was given the same probability. The predicted most probable Mn–Mn distance was 2.7 nm with a distribution of 0.5 nm at fwhh (Figure 2E). Similarly, starting from the X-ray structure of bis-TEMPO-OPE, its rotamers were generated and each was given the same probability. The predicted most probable spin–spin distance was 3.0 nm with a distribution of 0.1 nm at fwhh (Figure 3F).

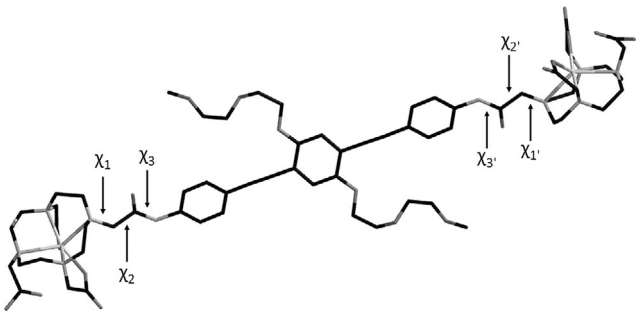

Figure 4. Schematic structure of $MnDOTA_2OPE$. The relevant dihedral angles, χ, of rotatable bonds of each MnDOTA are labeled. Hydrogen atoms have been omitted for clarity.

3. Discussion

The distance determined in the Q-band PELDOR measurements on bis-TEMPO-OPE **19** was in good agreement with that obtained from X-ray crystallography by using the point-dipole approximation and rotamer analysis. The strong orientation selection effect observed in the PELDOR time traces at these frequencies highlighted the rigidity of the molecule (and correspondingly of the OPE spacer). The determined width of the distance distribution profile was very narrow and could be attributed to bending of the OPE spacer and rotations of the single bonds of the molecule. This profile was in agreement with the prediction that had a sampling inaccuracy of 0.1 nm, but did not take into account bending of the molecule.

Compared with the bis-TEMPO-OPE results, the Mn–Mn distance obtained in W-band PELDOR measurements on $Mn\text{-}DOTA_2OPE$ were around six times more distributed. The bulk of this broadening was unlikely to have arisen from the bending of the OPE, but rather was most likely to be due to the inherent flexibility of the MnDOTA spin label. Indeed, the Mn–Mn distance distribution predicted by using a rotamer analysis was remarkably in reasonable agreement with the experimental data. Compared with PELDOR results, the predicted distance distribution profile was slightly shifted to longer distances; this was possibly due to sampling inaccuracy and/or inaccuracy of the method of modeling, such as 1) rotamer analysis did not take into account the small bending flexibility of the OPE spacer, which would give slightly shorter Mn–Mn distances; and 2) a dynamic coordination process in which the amide O atom coordinates to the Mn^{II} center,[80] which would favor shorter Mn–Mn distances. Alternatively, the differences between the experimental and predicted distance distribution profiles might also have originated from experimental data analysis, which did not take into account the pseudosecular term of the dipolar coupling Hamiltonian. For specific cases, in previous MnDOTA polyproline studies, this approach resulted in extra features at shorter distances.[27] The small feature at around 3.3 nm in the distance distribution profile, obtained in the PELDOR experiment, is possibly due to uncertainty in determining the background. Nevertheless, overall, the $MnDOTA_2OPE$ PELDOR results closely matched expectations, which suggested that MnDOTA spin labels could be used for measuring nanometric distances with relatively narrow distributions predictably, even at distances as short as 2.6 nm. Compared with the OPE spacer alone, each MnDOTA spin label only contributed around 0.3 nm to the distance and 0.3 nm to the distribution at fwhh. Although relatively small, the size and flexibility of the tethering DOTA arm appeared to outweigh the contribution from the pseudosecular term of the dipolar coupling Hamiltonian during Tikhonov regularization analysis. These advantages can potentially be further exploited by affixing MnDOTA to the biomolecule of interest in a more constrained manner, for example, by using 2,2′,2″-(10-{2-[(2,5-dioxopyrrolidin-1-yl)oxy]-2-oxoethyl}-1,4,7,10-tetraazacyclododecane-1,4,7-triyl)triacetic acid (DOTA-NHS ester), the protein backbone can be directly labeled at the N terminus,[81] or by using a derivative with short thiol-reactive tethers, similar to the Gd^{III} complexes very recently reported by Abdelkader et al.[79]

4. Conclusions

A model system incorporating two DOTA ligands on a short OPE spacer was designed, synthesized, and fully characterized. PELDOR measurements were performed on the corresponding Mn^{II} complex and on a bis-nitroxide analogue. The experimental Mn–Mn distance distribution obtained by Tikhonov regula-

rization was in good agreement with that simulated by using a simple rotamer analysis. However, there were small deviations, which might have arisen from a combination of shortcomings in the modeling and data analysis. Overall, our results suggested that PELDOR measurements with MnDOTA spin labels directly grafted on an object of interest could be used to determine nanometer distances with relatively narrow distributions predictably. Currently, we are studying the potential use of other MnDOTA derivatives as spin labels for PELDOR, as well as other dipolar EPR spectroscopic methods for Mn^{II}–Mn^{II} nanometer distance measurements, and these results will be reported in due course.

Experimental Section

Material and methods

^1H and ^{13}C NMR spectra were recorded on Bruker Avance 300 or 600 (300 or 400 MHz) spectrometers at the Ecole Normale Supérieure (ENS) in the Laboratoire des Biomolécules (LBM, UMR 7203) or at UPMC (Université Pierre et Marie Curie) in IPCM (Institut Parisien de Chimie Moléculaire, UMR 7201), with residual solvent signals as internal references. The following abbreviations were used: singlet (s), doublet (d), triplet (t), multiplet (m) and broad (br); δ indicates chemical shifts in ppm, J are coupling constants in Hz, and C_q are quaternary carbons. HRMS by using electrospray ionization (ESI) or atmospheric pressure chemical ionization (APCI) methods was performed at the Université Paris Sud in the Service de Spectrométrie de masse of the ICMMO (Institut de Chimie Moléculaire et des Matériaux d'Orsay). ESI-HRMS was also performed at UPMC (IPCM). MALDI-TOF MS was performed at UPMC in the Plate-forme de Spectrométrie de masse et Protéomique. The matrix was a saturated solution of α-cyano-4-hydroxycinnamic acid (HCCA) in MeCN/H_2O 1:1 with 0.1% TFA. Analytical TLC analysis was performed on silica gel plates (Merck 60F-254) with UV visualization at $\lambda = 254$ and 366 nm. Preparative column chromatography was performed with Merck silica gel (Si 60, 40–63 μm). Analytical HPLC measurements were performed on a Dionex Ultimate 3000 instrument by using C18A ACE columns. Preparative HPLC was performed on a Waters 600 instrument by using an XBridgeTM Prep C18 OBDTM column. Gradients of MeCN in H_2O, both containing 0.1% TFA, were employed. Products were monitored with UV detection. Unless otherwise stated, all syntheses were performed under an inert atmosphere (argon or nitrogen). Reagents and chemicals were purchased from Sigma–Aldrich, Alfa Aesar, Strem Chemicals, or Chematech. Dry solvents (CH_2Cl_2, MeCN, toluene, THF, dioxane, DMF, DMSO) were purchased from Sigma and used without further purification. EtOAc and triethylamine were dried with CaH_2, distilled under argon, and stored over 4 Å molecular sieves under argon.

2-(2-Methoxyethoxy)ethyl 4-methylbenzenesulfonate (2)

Compound **1** (39.1 mL, 332.7 mmol, 1.0 equiv) was dissolved in THF (110 mL). The resulting solution was cooled to 0 °C and NaOH (26.44 g, 661.0 mmol, 2.0 equiv) dissolved in H_2O (110 mL) was added dropwise, followed by TsCl (95.16 g, 499.0 mmol, 1.5 equiv) dissolved in THF (110 mL) dropwise. The resulting mixture was stirred at RT for 2 h and H_2O (400 mL) was added. The organic layer was recovered and washed without shaking with a 1 M aqueous solution of NaOH (2×) and H_2O (1×), dried over Na_2SO_4, filtered, and concentrated to afford **2** (72.95 g, 266.2 mmol, 80%) as a colorless oil. ^1H NMR ($CDCl_3$, 300 MHz): $\delta = 7.80$ (d, 2H, $J = 8.0$ Hz), 7.34 (d, 2H, $J = 8.0$ Hz), 4.17 (t, 2H, $J = 4.8$ Hz), 3.69 (t, 2H, $J = 4.8$ Hz), 3.61–3.54 (m, 2H), 3.51–3.44 (m, 2H), 3.35 (s, 3H), 2.44 ppm (s, 3H); ^{13}C NMR ($CDCl_3$, 75 MHz): $\delta = 144.9$ (C_q), 133.0 (C_q), 129.9 (CH), 128.1 (CH), 71.9 (CH_2), 70.8 (CH_2), 69.3 (CH_2), 68.8 (CH_2), 59.2 (CH_3), 21.8 ppm (CH_3); HRMS (ESI): m/z calcd for $C_{12}H_{19}O_5S^+$ $[M+H]^+$, $C_{12}H_{18}NaO_5S^+$ $[M+Na]^+$: 275.0948, 297.0766; found: 275.0950, 297.0767.

1,4-Bis[2-(2-methoxyethoxy)ethoxy]benzene (3)

Hydroquinone (14.64 g, 133.1 mmol, 1.0 equiv) and K_2CO_3 (73.47 g, 532.4 mmol, 4.0 equiv) were suspended in MeCN (1.1 L). The resulting suspension was heated at reflux for 30 min and cooled to RT. Compound **2** (72.95 g, 266.2 mmol, 2.0 equiv) dissolved in MeCN (220 mL) was added dropwise. The resulting mixture was heated at reflux for 72 h, cooled to RT, filtered, and concentrated. Column chromatography (SiO_2, cyclohexane/EtOAc 90:10 to 50:50) afforded **3** (32.81 g, 104.5 mmol, 79%) as an orange oil. ^1H NMR ($CDCl_3$, 300 MHz): $\delta = 6.83$ (s, 4H), 4.11–4.05 (m, 4H), 3.86–3.80 (m, 4H), 3.74–3.68 (m, 4H), 3.60–3.54 (m, 4H), 3.39 ppm (s, 6H); ^{13}C NMR ($CDCl_3$, 75 MHz): $\delta = 153.2$ (C_q), 115.6 (CH), 72.1 (CH_2), 70.9 (CH_2), 70.0 (CH_2), 68.1 (CH_2), 59.2 ppm (CH_3); HRMS (ESI): m/z calcd for $C_{16}H_{27}O_6^+$ $[M+H]^+$, $C_{16}H_{26}NaO_6^+$ $[M+Na]^+$; 315.1802, 337.1622; found: 315.1796, 337.1617.

1,4-Diiodo-2,5-bis[2-(2-methoxyethoxy)ethoxy]benzene (4)

Compound **3** (25.0 g, 79.6 mmol, 1.0 equiv), iodine (22.3 g, 87.6 mmol, 1.1 equiv), and KIO_3 (6.8 g, 31.8 mmol, 0.4 equiv) were dissolved in glacial AcOH (250 mL) and H_2O (25 mL). Concentrated H_2SO_4 (3.3 mL) was added, the resulting mixture was heated at reflux for 48 h and cooled to RT. CH_2Cl_2 and a 10% aqueous solution of $Na_2S_2O_3$ were added, the organic layer was recovered and washed with a saturated aqueous solution of $NaHCO_3$ (1×), H_2O (1×), and a saturated aqueous solution of NaCl (1×); dried over Na_2SO_4; filtered; and concentrated. Recrystallization from EtOH afforded **4** (27.27 g, 48.1 mmol, 60%) as a white solid. ^1H NMR ($CDCl_3$, 300 MHz): $\delta = 7.23$ (s, 2H), 4.14–4.07 (m, 4H), 3.92–3.86 (m, 4H), 3.80–3.74 (m, 4H), 3.61–3.55 (m, 4H), 3.40 ppm (s, 6H); ^{13}C NMR ($CDCl_3$, 75 MHz): $\delta = 153.2$ (C_q), 123.6 (CH), 86.5 (C_q), 72.2 (CH_2), 71.2 (CH_2), 70.5 (CH_2), 69.8 (CH_2), 59.3 ppm (CH_3); HRMS (ESI): m/z calcd for $C_{16}H_{25}I_2O_6^+$, $[M+H]^+$, $C_{16}H_{24}I_2NaO_6^+$ $[M+Na]^+$: 566.9735, 588.9554; found: 566.9707, 588.9544.

4,4′-({2,5-Bis[2-(2-methoxyethoxy)ethoxy]-1,4-phenylene}-bis(ethyne-2,1-diyl))dianiline (OPE-NH_2 6)

Compounds **4** (2.78 g, 5.0 mmol, 1.0 equiv) and **5** (1.17 g, 10.0 mmol, 2.0 equiv) were dissolved in dry THF (20 mL) and dry triethylamine (20 mL). Argon was bubbled for 15 min and $[Pd(PPh_3)_2Cl_2]$ (351.0 mg, 0.5 mmol, 0.1 equiv) and CuI (191.0 mg, 1.0 mmol, 0.2 equiv) were added. The resulting suspension was stirred for 24 h at RT; a saturated aqueous solution of NH_4Cl was added and the mixture was extracted with CH_2Cl_2 (3×). The combined organic layers were dried over Na_2SO_4, filtered, and concentrated. Column chromatography (SiO_2, 50:50 cyclohexane/EtOAc to 100% EtOAc) afforded **6** (1.41 g, 2.59 mmol, 52%) as an orange solid. ^1H NMR ($CDCl_3$, 300 MHz): $\delta = 7.32$ (d, $J = 8.4$ Hz, 4H), 6.99 (s, 2H), 6.63 (d, $J = 8.4$ Hz, 4H), 4.20 (t, $J = 5.0$ Hz, 4H), 3.92 (t, $J = 5.0$ Hz, 4H), 3.86–3.77 (m, 8H), 3.57–3.50 (m, 4H), 3.36 ppm (s, 6H); ^{13}C NMR ($CDCl_3$, 75 MHz): $\delta = 153.5$ (C_q), 146.9 (C_q), 133.1 (CH), 117.5

(CH), 114.9 (CH), 114.5 (C_q), 112.9 (C_q), 95.1 (C_q), 84.0 (C_q), 72.2 (CH_2), 71.2 (CH_2), 69.9 (CH_2), 69.9 (CH_2), 59.2 ppm (CH_3); HRMS (ESI): *m/z* calcd for $C_{32}H_{37}N_2O_6^+$ $[M+H]^+$, $C_{32}H_{36}N_2NaO_6^+$ $[M+Na]^+$: 545.2646, 567.2466; found: 545.2609, 567.2443.

N,N′-[({2,5-Bis[2-(2-methoxyethoxy)ethoxy]-1,4-phenylene}-bis(ethyne-2,1-diyl))bis(4,1-phenylene)]bis(2-bromoacetamide) (7)

OPE-NH_2 **6** (798 mg, 1.465 mmol, 1.0 equiv) was dissolved in dry CH_2Cl_2 (20 mL). The resulting solution was cooled to 0 °C, and triethylamine (496 μL, 3.66 mmol, 2.5 equiv) was added, followed by the dropwise addition of bromoacetyl bromide (319 μL, 3.66 mmol, 2.5 equiv) dissolved in dry CH_2Cl_2 (3 mL). The resulting mixture was allowed to warm to RT for 3 h and washed with a saturated aqueous solution of $NaHCO_3$ (1×) and a saturated aqueous solution of NaCl (1×). The organic layer was dried over Na_2SO_4, filtered, and concentrated. Compound **7** (459 mg, 0.584 mmol, 40%) was obtained after column chromatography (SiO_2, 40:60 to 20:80 cyclohexane/EtOAc) as a pale yellow solid. ^{1}H NMR ($CDCl_3$, 300 MHz): $\delta = 8.17$ (s, 2H), 7.59–7.48 (m, 8H), 7.03 (s, 2H), 4.22 (t, $J = 4.8$ Hz, 4H), 4.04 (s, 4H), 3.93 (t, $J = 4.8$ Hz, 4H), 3.83–3.78 (m, 4H), 3.57–3.52 (m, 4H), 3.37 ppm (s, 6H); ^{13}C NMR ($CDCl_3$, 75 MHz): $\delta = 163.4$ (C_q), 153.7 (C_q), 137.1 (C_q), 132.6 (CH), 120.1 (C_q), 119.7 (CH), 117.6 (CH), 114.3 (C_q), 94.7 (C_q), 86.0 (C_q), 72.2 (CH_2), 71.2 (CH_2), 69.9 (CH_2), 69.8 (CH_2), 59.2 (CH_3), 29.6 ppm (CH_2); HRMS (ESI): *m/z* calcd for $C_{36}H_{38}Br_2N_2NaO_8^+$ $[M+Na]^+$: 809.0867; found: 809.0859.

General Procedure A: Synthesis of Protected Bis-DOTA Compounds

Bromide **7** (1.0 equiv) and a DO3A derivative (tri-*t*Bu-DO3A or tri-Pp-DO3A **11**) (2.5 equiv) were mixed in dry MeCN. K_2CO_3 (10.0 equiv) was added and the resulting mixture was heated at 60 °C for 15 h and concentrated. CH_2Cl_2 was added and the mixture was washed with H_2O (1×) and a saturated aqueous solution of NaCl (1×). The organic layer was dried over Na_2SO_4, filtered, and concentrated. Column chromatography afforded the corresponding protected bis-DOTA-OPE compound as a yellow solid.

*t*Bu-Protected Bis-DOTA-OPE (8)

By using general procedure A with **7** (55 mg, 0.07 mmol), tri-*t*Bu-DO3A (100 mg, 0.174 mmol), and K_2CO_3 (96 mg, 0.7 mmol) in dry MeCN (10 mL), *t*Bu-protected bis-DOTA-OPE **8** (96 mg, 0.058 mmol, 83%) was obtained after column chromatography (SiO_2, 90:10 to 80:20 CH_2Cl_2/MeOH). ^{1}H NMR ($CDCl_3$, 300 MHz): $\delta = 11.49$ (s, 2H), 7.97 (d, $J = 8.5$ Hz, 4H), 7.34 (d, $J = 8.5$ Hz, 4H), 7.01 (s, 2H), 4.19 (t, $J = 5.0$ Hz, 4H), 3.91 (t, $J = 5.0$ Hz, 4H), 3.83–3.78 (m, 4H), 3.75 (s, 4H), 3.55–3.50 (m, 4H), 3.34 (s, 6H), 3.30–1.85 (m, 44H), 1.48 (s, 18H), 1.43 ppm (s, 36H); ^{13}C NMR ($CDCl_3$, 75 MHz): $\delta = 172.34$ (C_q), 171.6 (C_q), 153.6 (C_q), 140.1 (C_q), 131.8 (CH), 120.2 (CH), 117.6 (C_q), 114.5 (C_q), 95.9 (C_q), 84.7 (C_q), 82.4 (C_q), 82.2 (C_q), 72.2 (CH_2), 71.2 (CH_2), 69.9 (CH_2), 69.9 (CH_2), 59.1 (CH_3), 57.0 (CH_2), 55.9 (CH_2), 55.8 (CH_2), 51.3 (CH_2), 28.2 (CH_3), 28.1 ppm (CH_3); HRMS (ESI): *m/z* calcd for $C_{88}H_{136}N_{10}NaO_{20}^+$ $[M+Na]^+$: 1675.9825; found: 1675.9832.

2-Phenylpropan-2-yl 2-Bromoacetate (10)

Bromoacetic acid (10.0 g, 72 mmol, 1.0 equiv) and **9** (14.8 g, 109 mmol, 1.5 equiv) were dissolved in CH_2Cl_2 (100 mL). DMAP (880 mg, 7.2 mmol, 0.1 equiv) was added and the resulting mixture was cooled to 0 °C. DCC (15.2 g, 74 mmol, 1.03 equiv) was added portionwise and the resulting suspension was allowed to warm to RT for 3 h, filtered, and washed with CH_2Cl_2. The filtrate was washed with a 0.5 M aqueous solution of HCl (2×) and a saturated aqueous solution of $NaHCO_3$ (1×). The organic layer was dried over Na_2SO_4, filtered, and concentrated. Column chromatography (SiO_2, 95:5 cyclohexane/EtOAc) afforded **10** (10.82 g, 42.1 mmol, 58%) as a yellow oil. ^{1}H NMR ($CDCl_3$, 300 MHz): $\delta = 7.47$–7.24 (m, 5H), 3.80 (s, 2H), 1.84 ppm (s, 6H); ^{13}C NMR ($CDCl_3$, 100 MHz): $\delta = 165.1$ (C_q), 144.6 (C_q), 128.1 (CH), 127.0 (CH), 123.9 (CH), 83.4 (C_q), 28.0 (CH_3), 27.0 ppm (CH_2); HRMS (ESI): *m/z* calcd for $C_{11}H_{13}BrNaO_2^+$ $[M+Na]^+$: 278.9991; found: 278.9992.

Tris(2-phenylpropan-2-yl) 2,2′,2″-(1,4,7,10-Tetraazacyclododecane-1,4,7-triyl)triacetate (tri-Pp-DO3A 11)

Cyclen (2.41 g, 14 mmol, 1.0 equiv) was dissolved in MeCN (150 mL). The resulting solution was cooled to 0 °C and $NaHCO_3$ (3.53 g, 42 mmol, 3.0 equiv) was added. Compound **10** (10.8 g, 42 mmol, 3.0 equiv) dissolved in MeCN (40 mL) was added dropwise (≈30 min). The resulting suspension was allowed to warm to RT for 15 h and concentrated. CH_2Cl_2 was added and the mixture was washed with H_2O (1×) and a saturated aqueous solution of NaCl (1×). The organic layer was dried over Na_2SO_4, filtered, and concentrated. Column chromatography (SiO_2, 98:2 to 95:5 CH_2Cl_2/MeOH) afforded **11** (2.21 g, 3.15 mmol, 24%) as a light brown foam. ^{1}H NMR ($CDCl_3$, 300 MHz): $\delta = 9.82$ (s, 1H), 7.37–7.20 (m, 15H), 3.40–3.35 (m, 4H), 3.31 (s, 2H), 3.06–2.97 (m, 4H), 2.85–2.72 (m, 12H), 1.78 (s, 12H), 1.77 ppm (s, 6H); ^{13}C NMR ($CDCl_3$, 100 MHz): $\delta = 170.3$ (C_q), 169.3 (C_q), 145.4 (C_q), 145.2 (C_q), 128.5 (CH), 127.5 (CH), 127.4 (CH), 124.4 (CH), 124.4 (CH), 82.9 (C_q), 82.8 (C_q), 57.9 (CH_2), 52.1 (CH_2), 51.8 (CH_2), 49.7 (CH_2), 49.3 (CH_2), 47.3 (CH_2), 28.8 (CH_3), 28.8 ppm (CH_3); HRMS (ESI): *m/z* calcd for $C_{41}H_{57}N_4O_6^+$ $[M+H]^+$, $C_{41}H_{56}N_4NaO_6^+$ $[M+Na]^+$: 701.4273, 723.4092; found: 701.4315, 723.4096.

Pp-Protected Bis-DOTA-OPE (12)

By using general procedure A with **7** (71 mg, 0.09 mmol), **11** (161 mg, 0.23 mmol), and K_2CO_3 (124 mg, 0.9 mmol) in dry MeCN (8 mL), Pp-protected bis-DOTA-OPE **12** (99 mg, 0.049 mmol, 54%) was obtained after column chromatography (SiO_2, 95:5 to 85:15 CH_2Cl_2/MeOH). ^{1}H NMR ($CDCl_3$, 300 MHz): $\delta = 10.95$ (s, 2H), 7.91 (d, $J = 8.4$ Hz, 4H), 7.39 (d, $J = 8.4$ Hz, 4H), 7.34–7.08 (m, 30H), 7.04 (s, 2H), 4.21 (t, $J = 4.9$ Hz, 4H), 3.92 (t, $J = 4.9$ Hz, 4H), 3.84–3.76 (m, 4H), 3.56–3.49 (m, 4H), 3.34 (s, 6H), 3.25–1.95 (m, 44H), 1.62 ppm (s, 36H); ^{13}C NMR ($CDCl_3$, 100 MHz): $\delta = 171.6$ (C_q), 171.0 (C_q), 153.6 (C_q), 145.7 (C_q), 140.1 (C_q), 131.8 (CH), 128.4 (CH), 127.2 (CH), 124.2 (CH), 124.1 (CH), 120.1 (CH), 117.6 (CH), 117.4 (C_q), 114.5 (C_q), 95.9 (C_q), 84.8 (C_q), 83.4 (C_q), 83.3 (C_q), 72.2 (CH_2), 71.2 (CH_2), 69.9 (CH_2), 59.1 (CH_3), 56.6 (CH_2), 55.8 (CH_2), 55.7 (CH_2), 54–50.5 (CH_2, broad cluster), 50–47.5 (CH_2, broad cluster), 33–24 ppm (CH_3, broad cluster); HRMS (ESI): *m/z* calcd for $C_{118}H_{148}N_{10}Na_2O_{20}^{2+}/2$ $[M+2Na]^{2+}$, $C_{118}H_{149}N_{10}NaO_{20}^{2+}/2$ $[M+H+Na]^{2+}$: 1035.5328, 1025.0435; found: 1035.5329, 1025.0453.

Bis-DOTA-OPE (13)

Pp-protected bis-DOTA-OPE **12** was dissolved in a mixture of TFA/TIS/CH_2Cl_2 (2:2:96, 10 mg mL^{-1}). The resulting solution was stirred at RT for 4 h and concentrated. MeOH was added and the product was precipitated by slow addition of Et_2O, filtered, and dried. The

crude product was purified by preparative HPLC (30 to 50% MeCN) to afford bis-DOTA-OPE **13** as a yellow solid. HPLC: 5.02 min (5 to 100% MeCN in 10 min, >98%); MALDI-TOF MS (HCCA): *m/z* calcd for $C_{64}H_{89}N_{10}O_{20}^+$ $[M+H]^+$: 1317.62; found: 1317.43.

$MnDOTA_2OPE$

The Mn^{II} complex of bis-DOTA-OPE (**13**) was generated in situ for mass spectrometry analysis by the addition of $Mn(ClO_4)_2$ (2.0 equiv) to a buffered solution (HEPES 100 mM, pH 7.5) of **13**. MALDI-TOF MS (HCCA): *m/z* (%): 1423.46 (100) [Bis-DOTA-OPE−3H+2Mn]$^+$.

4-[(Trimethylsilyl)ethynyl]benzaldehyde (15)

Compound **14** (10.0 g, 54.05 mmol, 1.0 equiv) was dissolved in dry THF (40 mL) and dry triethylamine (20 mL). $[Pd(PPh)_3Cl_2]$ (380 mg, 0.541 mmol, 0.01 equiv) and CuI (103.3 mg, 0.541 mmol, 0.01 equiv) were added, and argon was bubbled for 15 min. TMSA (9.2 mL, 64.86 mmol, 1.2 equiv) was added dropwise and the resulting mixture was heated at reflux for 24 h and then cooled to RT. CH_2Cl_2 (200 mL) was added, the organic layer was recovered and washed with H_2O (1×), a 10% aqueous solution of HCl (1×), and H_2O (1×); dried over Na_2SO_4; filtered; and concentrated. Column chromatography (SiO_2, 100:0 to 90:10 cyclohexane/EtOAc) afforded **15** (9.31 g, 46.02 mmol, 85%) as a yellow solid. ^{1}H NMR ($CDCl_3$, 300 MHz): δ = 9.99 (s, 1H), 7.81 (d, 2H, J = 8.3 Hz), 7.60 (d, 2H, J = 8.3 Hz), 0.27 ppm (s, 9H); ^{13}C NMR ($CDCl_3$, 75 MHz): δ = 191.5 (CH), 135.7 (C_q), 132.6 (CH), 129.6 (CH), 129.5 (C_q), 104.0 (C_q), 99.2 (C_q), 0.1 ppm (CH_3); HRMS (ESI): *m/z* calcd for $C_{12}H_{15}OSi^+$ $[M+H]^+$, $C_{12}H_{14}NaOSi^+$ $[M+Na]^+$: 203.0887, 225.0706; found: 203.0886, 225.0668.

4-Ethynylbenzaldehyde (16)

Compound **15** (9.31 g, 46.02 mmol, 1.0 equiv) was dissolved in MeOH (450 mL). K_2CO_3 (4.77 g, 34.5 mmol, 0.75 equiv) was added and the resulting suspension was stirred at RT for 30 min. A saturated aqueous solution of NH_4Cl was added and the mixture was extracted with CH_2Cl_2 (3×). The combined organic layers were washed with H_2O (1×), dried over Na_2SO_4, filtered, and concentrated. Column chromatography (SiO_2, 100:0 to 90:10 cyclohexane/EtOAc) afforded **16** (5.87 g, 45.12 mmol, 98%) as a brown solid. ^{1}H NMR ($CDCl_3$, 300 MHz): δ = 10.02 (s, 1H), 7.87–7.81 (m, 2H), 7.67–7.60 (m, 2H), 3.29 ppm (s, 1H); ^{13}C NMR ($CDCl_3$, 75 MHz): δ = 191.5 (CH), 136.1 (C_q), 132.9 (CH), 129.6 (CH), 128.5 (C_q), 82.8 (C_q), 81.2 ppm (CH); HRMS (APCI): *m/z* calcd for $C_6H_7O_9^+$ $[M+H]^+$: 131.0491; found: 131.0493.

4,4′-({2,5-Bis[2-(2-methoxyethoxy)ethoxy]-1,4-phenylene}bis(ethyne-2,1-diyl))dibenzaldehyde (OPE-diCHO 17)

Compounds **4** (639 mg, 1.15 mmol, 1.0 equiv) and **16** (300 mg, 2.31 mmol, 2.0 equiv) were dissolved in dry THF (5 mL) and dry triethylamine (5 mL). Argon was bubbled for 15 min and then $[Pd(PPh_3)_2Cl_2]$ (81 mg, 0.115 mmol, 0.1 equiv) and CuI (44 mg, 0.23 mmol, 0.2 equiv) were added. The resulting suspension was stirred for 24 h at RT; a saturated aqueous solution of NH_4Cl was added and the mixture was extracted with CH_2Cl_2 (3×). The combined organic layers were dried over Na_2SO_4, filtered, and concentrated. Column chromatography (SiO_2, 80:20 to 0:100 cyclohexane/EtOAc) afforded OPE-diCHO **17** (528 mg, 0.925 mmol, 80%) as an orange solid. ^{1}H NMR ($CDCl_3$, 300 MHz): δ = 10.03 (s, 2H), 7.91–7.84 (m, 4H), 7.72–7.64 (m, 4H), 7.08 (s, 2H), 4.27- 4.21 (m, 4H), 3.98–3.92 (m, 4H), 3.83–3.77 (m, 4H), 3.58–3.53 (m, 4H), 3.37 ppm (s, 6H); ^{13}C NMR ($CDCl_3$, 75 MHz): δ = 191.4 (CH), 153.9 (C_q), 135.6 (C_q), 132.2 (CH), 129.7 (CH), 129.6 (C_q), 117.5 (CH), 114.3 (C_q), 94.5 (C_q), 89.9 (C_q), 72.1 (CH_2), 71.2 (CH_2), 69.9 (CH_2), 69.7 (CH_2), 59.2 ppm (CH_3); HRMS (ESI): *m/z* calcd for $C_{34}H_{35}O_8^+$ $[M+H]^+$, $C_{34}H_{34}NaO_8^+$ $[M+Na]^+$: 571.2326, 593.2146; found: 571.2315, 593.2134.

4,4′-({2,5-Bis[2-(2-methoxyethoxy)ethoxy]-1,4-phenylene}bis(ethyne-2,1-diyl))dibenzoic acid (OPE-diCO_2H 18)

OPE-diCHO **17** (1.5 g, 2.63 mmol, 1.0 equiv) was suspended in dry DMF (65 mL). $KHSO_5{\cdot}KHSO_4{\cdot}K_2SO_4$ (Oxone®; 3.23 g, 5.26 mmol, 2.0 equiv) was added and the resulting suspension was stirred at RT for 24 h. H_2O was added and the resulting precipitate was filtered and dried to afford OPE-diCO_2H **18** (1.294 g, 2.15 mmol, 82%) as a yellow solid. ^{1}H NMR ([D$_6$]DMSO, 300 MHz): δ = 13.13 (s, 2H), 8.03–7.94 (m, 4H), 7.68–7.60 (m, 4H), 7.27 (s, 2H), 4.20 (t, J = 4.5 Hz, 4H), 3.80 (t, J = 4.5 Hz, 4H), 3.71–3.64 (m, 4H), 3.48–3.41 (m, 4H), 3.21 ppm (s, 6H); ^{13}C NMR ([D$_6$]DMSO, 75 MHz): δ = 166.7 (C_q), 153.2 (C_q), 131.4 (CH), 130.6 (C_q), 129.6 (CH), 126.8 (C_q), 116.9 (CH), 113.1 (C_q), 94.3 (C_q), 88.8 (C_q), 71.4 (CH_2), 70.1 (CH_2), 69.1 (CH_2), 69.0 (CH_2), 58.1 ppm (CH_3); HRMS (ESI): *m/z* calcd for $C_{34}H_{33}O_{10}^-$ $[M-H]^-$, $C_{34}H_{32}O_{10}^{2-}/2$ $[M-2H]^{2-}$: 601.2079, 300.1003; found: 601.2076, 300.1022.

Bis-TEMPO-OPE (19)

OPE-diCO_2H **18** (57 mg, 0.094 mmol, 1.0 equiv) and 4-NH_2-TEMPO (40 mg, 0.234 mmol, 2.5 equiv) were dissolved in dry DMF (2 mL). The resulting solution was cooled to 0 °C, HOBt·H_2O (43 mg, 0.282 mmol, 3.0 equiv) and DCC (58 mg, 0.282 mmol, 3 equiv) were added, and the resulting mixture was stirred at RT for 24 h. H_2O was added and the mixture was extracted with CH_2Cl_2 (3×). The combined organic layers were dried over Na_2SO_4, filtered, and concentrated. Column chromatography (SiO_2, 30:70 to 20:80 cyclohexane/EtOAc) afforded bis-TEMPO-OPE **19** (79 mg, 0.087 mmol, 93%) as an orange solid. R_f (SiO_2): 0.39 (100% EtOAc); ^{1}H NMR ($CDCl_3$, 300 MHz; all signals broadened and some obscured due to paramagnetism): δ = 8.05–7.53 (m, 8H), 7.09 (s, 2H), 4.25 (br s, 4H), 3.96 (br s, 4H), 3.82 (br s, 4H), 3.57 (br s, 4H), 3.39 (s, 6H), 2.12–0.79 ppm (m, 32H); HPLC: 6.92 min (40 to 100% MeCN in 10 min, 95%); HRMS (ESI): *m/z* calcd for $C_{52}H_{69}N_4O_{10}^{2+}$ $[M+H]^{2+}$, $C_{52}H_{68}N_4NaO_{10}^{2+}$ $[M+Na]^{2+}$: 909.5008, 931.4828; found: 909.4968, 931.4793.

X-ray Crystallography

XRD data for compound **17** was collected by using a Kappa X8 APEX II Bruker diffractometer with graphite-monochromated MoKα radiation (λ = 0.71073 Å). XRD data for compound **19** was collected by using a Kappa VENTURE PHOTON 100 Bruker diffractometer with IμS microfocus graphite-monochromated MoKα radiation (λ = 0.71073 Å). Crystals were mounted on a CryoLoop (Hampton Research) with Paratone-N (Hampton Research) as a cryoprotectant and then flash frozen in a nitrogen gas stream at 100 K. The temperature of the crystal was maintained at the selected value (100 K) by means of a 700 series Cryostream cooling device to within an accuracy of ±1 K. The data were corrected for Lorentz polarization and absorption effects. The structures were solved by direct methods by using SIR-97[82] and refined against F^2 by full-matrix least-squares techniques by using SHELXL-2013[83] with anisotropic displacement parameters for all non-hydrogen atoms. All

calculations were performed by using the crystal structure crystallographic software package WINGX.[84]

The crystal data collection and refinement parameters are given in Table S1 in the Supporting Information.

The experimental data indicated positional static disorder of toluene of compound **19** (on inversion center). In the figures, the disordered toluene molecule is omitted for clarity.

CCDC 1431929-1431930 contains the supplementary crystallographic data for this paper. These data can be obtained free of charge from The Cambridge Crystallographic Data Centre.

EPR Measurements

W-band PELDOR measurements were performed on a Bruker Elexsys II 680 EPR spectrometer equipped with a Bruker "power upgrade 2" and an Oxford Instruments CF935 flow cryostat. For $MnDOTA_2OPE$ all experiments were performed at a sample temperature of 10 K. Spin-echo-detected EPR spectra were taken by using a Hahn-echo sequence with $\pi/2$ and π pulse durations of 12 and 24 ns, an interpulse delay time of 2500 ns, a shot repetition time of 800 μs, and a sweep width of 1000 G. For PELDOR measurements, the four-pulse, dead-time-free sequence[11,12] was used and the difference between the pump and detection frequencies was +70 MHz. The pump pulse duration was 24 ns and the duration of the $\pi/2$ and π detection pulses was 12 and 24 ns. The initial interpulse delay (between detection $\pi/2$ and π pulses) was 544 ns and the dipolar evolution window was 2226 ns. A four-step phase cycle procedure was used. The shot repetition time was 800 μs with 100 shots per point and the number of scans was 156, which equated to an accumulation time of 1.5 h. For bis-TEMPO-OPE **19**, all experiments were performed at a sample temperature of 40 K. Spin-echo-detected EPR spectra were recorded by using a Hahn-echo sequence with $\pi/2$ and π pulse durations of 40 and 80 ns, an interpulse delay time of 1500 ns, a shot repetition time of 5 ms, and a sweep width of 400 G. For PELDOR measurements, the difference between the pump and detection frequencies was +70 MHz. The pump pulse duration was 80 ns and the duration of the $\pi/2$ and π detection pulses was 40 and 80 ns. The initial interpulse delay (between detection $\pi/2$ and π pulses) was 400 ns and the dipolar evolution window was 1500 μs. A four-step phase cycle procedure was used. The shot repetition time was 5 ms with 100 shots per point and the number of scans was 25. The total accumulation time of the 3 PELDOR time traces was about 4.5 h.

Q-band PELDOR measurements were performed on a Bruker Elexsys E580 spectrometer, equipped with a 10 W AMP-Q-Band solid-state amplifier. A more detailed description of the Q-band setup is given elsewhere.[85] All experiments were performed with the ER5107D2 probe at a sample temperature of 50 K. Spin-echo-detected EPR spectra were recorded by using a Hahn-echo sequence with $\pi/2$ and π pulse durations of 16 and 32 ns, an interpulse delay time of 130 ns, a shot repetition time of 3 ms, and a sweep width of 140 G. For PELDOR measurements, the difference between the pump and detection frequencies was +50 or −50 MHz. The pump pulse duration was 22 ns and the duration of all detection pulses were 32 ns. The initial interpulse delay (between detection $\pi/2$ and π pulses) was 332 ns and the dipolar evolution window was 5 μs. To suppress deuterium modulations in the PELDOR time traces, the initial interpulse delay time was incremented by 16 ns over 8 steps (tau averaging procedure). A two-step phase cycle procedure was used. The shot repetition time was 3 ms with 20 shots per point and the number of scans was varied from 8 to 19, depending on the spectral position at which the PELDOR time traces were recorded. The accumulation time of the full set of PELDOR time traces was about 5 h.

Rotamer Analysis

Starting from the X-ray crystal structures of MnH_2DOTA[80] and the OPE spacer of bis-TEMPO-OPE **19**, a model of $MnDOTA_2OPE$ was constructed in Spartan 14 (Wavefunction Inc.) For the MnDOTA arm that linked each spin label to the OPE, dihedral angles for the C–N bond (χ_1 and $\chi_{1'}$) and C–C bond (χ_2 and $\chi_{2'}$) were restricted to staggered conformations. The values of χ_3 and $\chi_{3'}$ were fixed because previous studies showed that the acetanilide unit was overwhelmingly in the *trans* configuration.[86] Relative to each other, the two spin-labeled ends were allowed to fully rotate around the molecular axis in 30° intervals. From these parameters, all 972 possible rotamers were systematically generated and molecular mechanic force field calculations were performed on each to identify and eliminate those with clashes. For the remainder, 406 rotamers, each was given the same probability and the Mn–Mn distances were compiled in 0.1 nm boxes. Similarly, starting from the X-ray structure of bis-TEMPO-OPE, the dihedral angles of the rotatable C–N bonds were restricted to staggered conformations and, relative to each other, the two spin-labeled ends were allowed to fully rotate around the molecular axis in 30° intervals. From these parameters, all 108 possible clash-free rotamers were systematically generated. Each was given the same probability and the distances between the middle points of the N–O bonds were compiled in 0.1 nm boxes.

Acknowledgements

This work was financially supported by ANR MnHFPELDOR, ANR-DFG Chemistry 2011-INTB-1010-01 (P.D.-D. PhD studentship and H.Y.V.C. post-doctoral fellowship) and DFG (GZ: PR 294/14-1, D.A. PhD studentship). We thank the French Infrastructure for Integrated Structural Biology (FRISBI) for financial support. The W-band spectrometer was funded by the Région Ile-de-France "Sesame" program, the CEA, and CNRS. We thank UPS, IUF, Région Ile de France SESAME program 2012 no. 12018501, LabEx CHARM3AT, and CNRS for X-ray crystallography. We are very grateful to Dr. Sun Un (I2BC-CEA Saclay), Prof. Thomas Prisner (Goethe Universität Frankfurt), Dr. Burkhard Endeward (Goethe Universität Frankfurt), and Dr. Alice Bowen (Goethe Universität Frankfurt) for spectrometer access and fruitful and constructive discussions.

Keywords: EPR spectroscopy · gadolinium · manganese · pulsed electron–electron double resonance · spin labels

[1] J. R. Lakowicz, *Principles of Fluorescent Spectroscopy*, 3rd ed., Springer, New York, **2006**.
[2] M. Hong, K. Schmidt-Rohr, *Acc. Chem. Res.* **2013**, *46*, 2154–2163.
[3] H. D. T. Mertens, D. I. Svergun, *J. Struct. Biol.* **2010**, *172*, 128–141.
[4] O. Duss, M. Yulikov, G. Jeschke, F. H.-T. Allain, *Nat. Commun.* **2014**, *5*, 3669.
[5] R. R. Ernst, *Angew. Chem. Int. Ed. Engl.* **1992**, *31*, 805–823; *Angew. Chem.* **1992**, *104*, 817–836.
[6] K. Wüthrich, *Nat. Struct. Biol.* **2001**, *8*, 923–925.
[7] O. Schiemann, T. F. Prisner, *Q. Rev. Biophys.* **2007**, *40*, 1–53.
[8] G. Jeschke, *Annu. Rev. Phys. Chem.* **2012**, *63*, 419–446.

[9] Y. D. Tsvetkov, A. D. Milov, A. G. Maryasov, *Russ. Chem. Rev.* **2008**, *77*, 487 – 520.
[10] A. D. Milov, A. B. Ponomarev, Y. D. Tsvetkov, *Chem. Phys. Lett.* **1984**, *110*, 67 – 72.
[11] R. E. Martin, M. Pannier, F. Diederich, V. Gramlich, M. Hubrich, H. W. Spiess, *Angew. Chem. Int. Ed.* **1998**, *37*, 2833 – 2837; *Angew. Chem.* **1998**, *110*, 2993 – 2998.
[12] M. Pannier, S. Veit, A. Godt, G. Jeschke, H. W. Spiess, *J. Magn. Reson.* **2000**, *142*, 331 – 340.
[13] A. D. Milov, K. M. Salikhov, M. D. Shchirov, *Sov. Phys. Solid State* **1981**, *23*, 565 – 569; *Fiz. Tverd. Tela Leningrad* **1981**, *23*, 975 – 982.
[14] W. L. Hubbell, A. Gross, R. Langen, M. A. Lietzow, *Curr. Opin. Struct. Biol.* **1998**, *8*, 649 – 656.
[15] W. L. Hubbell, C. J. López, C. Altenbach, Z. Yang, *Curr. Opin. Struct. Biol.* **2013**, *23*, 725 – 733.
[16] Y. D. Tsvetkov, *J. Struct. Chem.* **2013**, *54*, 42 – 72.
[17] Y. Polyhach, E. Bordignon, R. Tschaggelar, S. Gandra, A. Godt, G. Jeschke, *Phys. Chem. Chem. Phys.* **2012**, *14*, 10762 – 10773.
[18] V. P. Denysenkov, T. F. Prisner, J. Stubbe, M. Bennati, *Proc. Natl. Acad. Sci. USA* **2006**, *103*, 13386 – 13390.
[19] Y. Polyhach, A. Godt, C. Bauer, G. Jeschke, *J. Magn. Reson.* **2007**, *185*, 118 – 129.
[20] O. Schiemann, P. Cekan, D. Margraf, T. F. Prisner, S. T. Sigurdsson, *Angew. Chem. Int. Ed.* **2009**, *48*, 3292 – 3295; *Angew. Chem.* **2009**, *121*, 3342 – 3345.
[21] A. M. Bowen, C. E. Tait, C. R. Timmel, J. R. Harmer, *Struct. Bonding (Berlin)* **2013**, *152*, 283 – 328.
[22] A. P. Jagtap, I. Krstic, N. C. Kunjir, R. Hänsel, T. F. Prisner, S. T. Sigurdsson, *Free Radical Res.* **2015**, *49*, 78 – 85.
[23] D. Goldfarb, *Struct. Bonding (Berlin)* **2014**, *152*, 164 – 203.
[24] D. Goldfarb, *Phys. Chem. Chem. Phys.* **2014**, *16*, 9685 – 9699.
[25] A. Feintuch, G. Otting, D. Goldfarb, *Methods Enzymol.* **2015**, *563*, 415 – 457.
[26] D. Banerjee, H. Yagi, T. Huber, G. Otting, D. Goldfarb, *J. Phys. Chem. Lett.* **2012**, *3*, 157 – 160.
[27] H. Y. V. Ching, P. Demay-Drouhard, H. C. Bertrand, C. Policar, L. C. Tabares, S. Un, *Phys. Chem. Chem. Phys.* **2015**, *17*, 23368 – 23377.
[28] A. Martorana, Y. Yan, Y. Zhao, Q.-F. Li, X.-C. Su, D. Goldfarb, *Dalton Trans.* **2015**, *44*, 20812 – 20816.
[29] A. M. Raitsimring, C. Gunanathan, A. Potapov, I. Efremenko, J. M. L. Martin, D. Milstein, D. Goldfarb, *J. Am. Chem. Soc.* **2007**, *129*, 14138 – 14139.
[30] A. Dalaloyan, M. Qi, S. Ruthstein, S. Vega, A. Godt, A. Feintuch, D. Goldfarb, *Phys. Chem. Chem. Phys.* **2015**, *17*, 18464 – 18476.
[31] A. Potapov, Y. Song, T. J. Meade, D. Goldfarb, A. V. Astashkin, A. Raitsimring, *J. Magn. Reson.* **2010**, *205*, 38 – 49.
[32] A. Potapov, H. Yagi, T. Huber, S. Jergic, N. E. Dixon, G. Otting, D. Goldfarb, *J. Am. Chem. Soc.* **2010**, *132*, 9040 – 9048.
[33] D. T. Edwards, T. Huber, S. Hussain, K. M. Stone, M. Kinnebrew, I. Kaminker, E. Matalon, M. S. Sherwin, D. Goldfarb, S. Han, *Structure* **2014**, *22*, 1677 – 1686.
[34] H. Yagi, D. Banerjee, B. Graham, T. Huber, D. Goldfarb, G. Otting, *J. Am. Chem. Soc.* **2011**, *133*, 10418 – 10421.
[35] E. H. Abdelkader, A. Feintuch, X. Yao, L. A. Adams, L. Aurelio, B. Graham, D. Goldfarb, G. Otting, *Chem. Commun.* **2015**, *51*, 15898 – 15901.
[36] M. Gordon-Grossman, I. Kaminker, Y. Gofman, Y. Shai, D. Goldfarb, *Phys. Chem. Chem. Phys.* **2011**, *13*, 10771 – 10780.
[37] E. Matalon, T. Huber, G. Hagelueken, B. Graham, V. Frydman, A. Feintuch, G. Otting, D. Goldfarb, *Angew. Chem. Int. Ed.* **2013**, *52*, 11831 – 11834; *Angew. Chem.* **2013**, *125*, 12047 – 12050.
[38] Y. Song, T. J. Meade, A. V. Astashkin, E. L. Klein, J. H. Enemark, A. Raitsimring, *J. Magn. Reson.* **2011**, *210*, 59 – 68.
[39] A. Martorana, G. Bellapadrona, A. Feintuch, M. Elbaum, E. Di Gregorio, S. Aime, D. Goldfarb, *J. Am. Chem. Soc.* **2014**, *136*, 13458 – 13465.
[40] M. Qi, A. Groß, G. Jeschke, A. Godt, M. Drescher, *J. Am. Chem. Soc.* **2014**, *136*, 15366 – 15378.
[41] F. Wojciechowski, A. Groß, I. T. Holder, L. Knörr, M. Drescher, J. S. Hartig, *Chem. Commun.* **2015**, *51*, 13850 – 13853.
[42] L. C. Tabares, J. Gätjens, C. Hureau, M. R. Burrell, L. Bowater, V. L. Pecoraro, S. Bornemann, S. Un, *J. Phys. Chem. B* **2009**, *113*, 9016 – 9025.
[43] C. W. Bock, A. K. Katz, G. D. Markham, J. P. Glusker, *J. Am. Chem. Soc.* **1999**, *121*, 7360 – 7372.
[44] G. Jeschke, V. Chechik, P. Ionita, A. Godt, H. Zimmermann, J. Banham, C. R. Timmel, D. Hilger, H. Jung, *Appl. Magn. Reson.* **2006**, *30*, 473 – 498.
[45] N. C. Kunjir, G. W. Reginsson, O. Schiemann, S. T. Sigurdsson, *Phys. Chem. Chem. Phys.* **2013**, *15*, 19673 – 19685.
[46] E. Brücher, G. Tircsó, Z. Baranyai, Z. Kovács, A. D. Sherry in *The Chemistry of Contrast Agents in Medical Magnetic Resonance Imaging*, 2nd ed. (Eds.: A. Merbach, L. Helm, E. Tóth), Wiley, Hoboken, **2013**.
[47] J. M. Tour, *Chem. Rev.* **1996**, *96*, 537 – 554.
[48] N. M. Jenny, M. Mayor, T. R. Eaton, *Eur. J. Org. Chem.* **2011**, 4965 – 4983.
[49] A. Godt, M. Schulte, H. Zimmermann, G. Jeschke, *Angew. Chem. Int. Ed.* **2006**, *45*, 7560 – 7564; *Angew. Chem.* **2006**, *118*, 7722 – 7726.
[50] G. Jeschke, M. Sajid, M. Schulte, N. Ramezanian, A. Volkov, H. Zimmermann, A. Godt, *J. Am. Chem. Soc.* **2010**, *132*, 10107 – 10117.
[51] A. Weber, O. Schiemann, B. Bode, T. F. Prisner, *J. Magn. Reson.* **2002**, *157*, 277 – 285.
[52] G. Jeschke, H. Zimmermann, A. Godt, *J. Magn. Reson.* **2006**, *180*, 137 – 146.
[53] G. W. Reginsson, N. C. Kunjir, S. T. Sigurdsson, O. Schiemann, *Chem. Eur. J.* **2012**, *18*, 13580 – 13584.
[54] D. Akhmetzyanov, P. Schöps, A. Marko, N. C. Kunjir, S. T. Sigurdsson, T. F. Prisner, *Phys. Chem. Chem. Phys.* **2015**, *17*, 24446 – 24451.
[55] Y. Zhao, Y. Shirai, A. D. Slepkov, L. Cheng, L. B. Alemany, T. Sasaki, F. A. Hegmann, J. M. Tour, *Chem. Eur. J.* **2005**, *11*, 3643 – 3658.
[56] H. Meier, D. Ickenroth, U. Stalmach, K. Koynov, A. Bahtiar, C. Bubeck, *Eur. J. Org. Chem.* **2001**, *2001*, 4431 – 4443.
[57] B. Sontag, M. Rüth, P. Spiteller, N. Arnold, W. Steglich, M. Reichert, G. Bringmann, *Eur. J. Org. Chem.* **2006**, *2006*, 1023 – 1033.
[58] N. Saini, R. Varshney, A. K. Tiwari, A. Kaul, M. Allard, M. P. S. Ishar, A. K. Mishra, *Dalton Trans.* **2013**, *42*, 4994 – 5003.
[59] M. Lee, M. S. Tremblay, S. Jockusch, N. J. Turro, D. Sames, *Org. Lett.* **2011**, *13*, 2802 – 2805.
[60] Y. O. Fung, W. Wu, C. T. Yeung, H. K. Kong, K. K. C. Wong, W. S. Lo, G. L. Law, K. L. Wong, C. K. Lau, C. S. Lee, W. T. Wong, *Inorg. Chem.* **2011**, *50*, 5517 – 5525.
[61] A. J. Wilkinson, D. Maffeo, A. Beeby, C. E. Foster, J. A. G. Williams, *Inorg. Chem.* **2007**, *46*, 9438 – 9449.
[62] J. Luo, W.-S. Li, P. Xu, L.-Y. Zhang, Z.-N. Chen, *Inorg. Chem.* **2012**, *51*, 9508 – 9516.
[63] J. Laakso, G. A. Rosser, C. Szíjjártó, A. Beeby, K. E. Borbas, *Inorg. Chem.* **2012**, *51*, 10366 – 10374.
[64] R. F. H. Viguier, A. N. Hulme, *J. Am. Chem. Soc.* **2006**, *128*, 11370 – 11371.
[65] M. Jamous, U. Haberkorn, W. Mier, *Molecules* **2013**, *18*, 3379 – 3409.
[66] W. Mier, K. A. N. Graham, Q. Wang, S. Krämer, J. Hoffend, M. Eisenhut, U. Haberkorn, *Tetrahedron Lett.* **2004**, *45*, 5453 – 5455.
[67] M. Jamous, U. Haberkorn, W. Mier, *Tetrahedron Lett.* **2012**, *53*, 6810 – 6814.
[68] C. Yue, J. Thierry, P. Potier, *Tetrahedron Lett.* **1993**, *34*, 323 – 326.
[69] Z. Wang, S. Yuan, A. Mason, B. Reprogle, D. J. Liu, L. Yu, *Macromolecules* **2012**, *45*, 7413 – 7419.
[70] S. Valera, J. E. Taylor, D. S. B. Daniels, D. M. Dawson, K. S. Athukorala Arachchige, S. E. Ashbrook, A. M. Z. Slawin, B. E. Bode, *J. Org. Chem.* **2014**, *79*, 8313 – 8323.
[71] C. F. Macrae, P. R. Edgington, P. McCabe, E. Pidcock, G. P. Shields, R. Taylor, M. Towler, J. van de Streek, *J. Appl. Crystallogr.* **2006**, *39*, 453 – 457.
[72] A. Marko, D. Margraf, H. Yu, Y. Mu, G. Stock, T. Prisner, *J. Chem. Phys.* **2009**, *130*, 064102.
[73] A. Marko, V. Denysenkov, D. Margraf, P. Cekan, O. Schiemann, S. T. Sigurdsson, T. F. Prisner, *J. Am. Chem. Soc.* **2011**, *133*, 13375 – 13379.
[74] A. Marko, T. F. Prisner, *Phys. Chem. Chem. Phys.* **2013**, *15*, 619 – 627.
[75] D. Abdullin, G. Hagelueken, R. I. Hunter, G. M. Smith, O. Schiemann, *Mol. Phys.* **2015**, *113*, 544 – 560.
[76] T. F. Prisner, A. Marko, S. T. Sigurdsson, *J. Magn. Reson.* **2015**, *252*, 187 – 198.
[77] G. Hagelueken, R. Ward, J. H. Naismith, O. Schiemann, *Appl. Magn. Reson.* **2012**, *42*, 377 – 391.
[78] G. Hagelueken, D. Abdullin, R. Ward, O. Schiemann, *Mol. Phys.* **2013**, *111*, 2757 – 2766.

[79] E. H. Abdelkader, M. D. Lee, A. Feintuch, M. Ramirez Cohen, J. D. Swarbrick, G. Otting, B. Graham, D. Goldfarb, *J. Phys. Chem. Lett.* **2015**, *6*, 5016 – 5021.
[80] S. Wang, T. D. Westmoreland, *Inorg. Chem.* **2009**, *48*, 719 – 727.
[81] G. Schwarz, L. Mueller, S. Beck, M. W. Linscheid, *J. Anal. At. Spectrom.* **2014**, *29*, 221 – 233.
[82] A. Altomare, M. C. Burla, M. Camalli, G. L. Cascarano, C. Giacovazzo, A. Guagliardi, A. G. Moliterni, G. Polidori, R. Spagna, *J. Appl. Crystallogr.* **1999**, *32*, 115 – 119.
[83] G. M. Sheldrick, *Acta Crystallogr. Sect. A* **2008**, *64*, 112 – 122.
[84] L. J. Farrugia, *J. Appl. Crystallogr.* **1999**, *32*, 837 – 838.
[85] P. Schöps, P. E. Spindler, A. Marko, T. F. Prisner, *J. Magn. Reson.* **2015**, *250*, 55 – 62.
[86] H. Kessler, A. Rikler, *Liebigs Ann. Chem.* **1967**, *708*, 57 – 68.

Manuscript received: March 7, 2016
Accepted Article published: March 27, 2016
Final Article published: ■■ ▮▮, 2016

P. Demay-Drouhard, H. Y. V. Ching, D. Akhmetzyanov, R. Guillot, L. C. Tabares, H. C. Bertrand, C. Policar**

■■ – ■■

A Bis-Manganese(II)–DOTA Complex for Pulsed Dipolar Spectroscopy

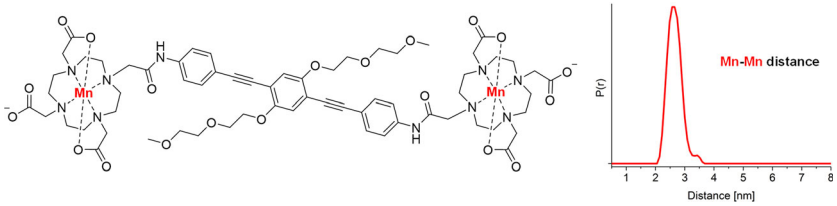

New labels for spin: The efficient synthesis of a model system consisting of two $[Mn(dota)]^{2-}$ ($DOTA^{4-}$ = 1,4,7,10-tetraazacyclododecane-1,4,7,10-tetraacetate; see figure) molecules directly connected to a central rodlike oligo(phenylene–ethynylene) spacer is described. This study illustrates the potential of these spin labels for measuring short nanometer distances.